Journal of Magnetic Resonance Open 14-15 (2023) 100086

Contents lists available at ScienceDirect

Journal of Magnetic Resonance Open

journal homepage: www.sciencedirect.com/journal/journal-of-magnetic-resonance-open

New challenges and opportunities for low-field MRI

Esteban Anoardo [*,a], Gonzalo G. Rodriguez [b]

[a] Laboratorio de Relaxometría y Técnicas Especiales (LaRTE), Grupo de Resonancia Magnética Nuclear, FaMAF - Universidad Nacional de Córdoba e IFEG-CONICET, Córdoba, Argentina

[b] Center for Biomedical Imaging, Department of Radiology, New York University, Grossman School of Medicine, New York, United States

ARTICLE INFO

Keywords:
MRI
Low-field
Pre-polarized
Field-cycling
Magnet

ABSTRACT

In this manuscript we deal with recent advances in low-field Magnetic Resonance Imaging (MRI). The development of low-cost MRI solutions allowing portability and trustable diagnosis is a hot topic worldwide by these days. We analyze basic technical issues of recent examples of fixed-field instruments operating at low-field. Then we discuss pros and cons of the pre-polarized approach, from both physical and technical perspectives. Permanent magnet and electromagnet technology are confronted. Finally, magnetic field-cycling is introduced as an alternative MRI technique, where field-dependent experiments can be exploded for the development of new contrast mechanisms that are not feasible for fixed-field MRI instruments. As field cycled machines usually deals with switched currents in electromagnets, magnetic field instability and inhomogeneity are the main limiting factors affecting image quality. We finalize this manuscript discussing how it turns possible to overcome these limitations, thus opening new possibilities for the development of cost effective MRI technology.

1. Introduction

MRI is mainly based on three pillars: hardware, contrast mechanisms and data post-processing. The evolution of electronic devices and magnetic materials allowed an important reduction of NMR instrumentation size and weight. Today one single chip can afford functionalities that in the past were distributed in several modules located in a 19" rack. Low-cost magnets allowed obtaining reasonable quality of images in non-uniform magnetic fields, while image distortions can be repaired using adequate post-processing correcting algorithms. No sophisticated computers (within the current state of the art) are required to run such corrections in times that are compatible with typical MRI experimental data acquisition times, which in turn can be reduced by using specific contrast mechanisms and appropriated pulse sequences. Today we know that a magnetic field intensity of at least 0.1 T, a field homogeneity of the order a few ppm (in large volumes compatible with whole-body MRI), and short-term magnetic field stability of the order of 0.1 ppm, do not represent strict requirements for MRI [1].

These facts have triggered in the last years an increasing interest for compact, portable, low-cost and efficient quality-to-cost diagnosis instruments. A main reason stimulating this increased activity in the field relies in the concrete possibility to popularize the access of MRI to a much larger population of potential patients. However, there is also a silent in-progress impact in education with astonishing possibilities for the training of engineering, radiology and biomedical sciences students, basic & applied research and industrial applications. A clear indicator of this potentiality is the recent appearance and expansion in the market of several MRI-tech companies dedicated to the development of low-field scanners. Hyperfine introduced in the market the first low-field brain scanner with FDA clearance [2]. Neuro42 in USA and DeepSpin in Germany are also developing dedicated head MRI low-field scanners, and PhysioMRI is developing a dedicated version for extremities in Spain.

Reducing the requirements regarding the maximum magnetic field intensity (B_0) has a global impact on the scanner design. The fact that $B_0 < 0.5$T can be generated without the need of super-conducting magnets strongly reduces the costs (cryogenic cooling systems are not needed) and provides high flexibility in the magnet design. Based on this fact, in this manuscript we will refer to "low-field" for MRI instruments operating at magnetic fields lower than 0.5 T.

In contrast to fixed-field instruments (mainly based today on permanent magnet arrays), we will also refer to pre-polarized technology. In this case, a higher magnetic field is used to boost-up the magnetization in order to gain signal-to-noise ratio (SNR) [3–6]. In the context of field-cycled approaches, special features of the fast field-cycling (FFC-MRI) technique will be mentioned. This variant offers a plenty of

* Corresponding author at: Famaf - UNC/IFEG - CONICET, Ciudad Universitaria, Córdoba, Argentina.
E-mail address: eanoardo@unc.edu.ar (E. Anoardo).

https://doi.org/10.1016/j.jmro.2022.100086
Received 6 September 2022; Received in revised form 29 November 2022; Accepted 2 December 2022
Available online 13 December 2022

possibilities for MRI which are forbidden or limited for fixed-field devices. Such possibilities arise from the fact that image construction can be performed after evolving or manipulating the spin system at different magnetic field intensities [7–11]. In these techniques, combined magnet technology is quite common, although the exclusive use of electromagnet systems may turn into an attractive alternative. In such a case, however, not only the magnetic field homogeneity turns relevant, but also the magnetic field stability. A main challenging situation for pure switchable electromagnet MRI (pre-polarized & field-cycled) relies in the underlying physics and engineering for a competitive quality-cost equation.

Fig. 1 resumes the evolution in the last years of the volume of publications as estimated using Scholar Google with the strings {"Halbach + magnet" AND "MRI"}, and {("prepolarized" OR "field-cycling") + "electromagnet" + "MRI"}. Although a rough estimation, the figure suggests a noticeable increase in the interest for Halbach magnets in the last two years. As we will see later, this tendency is supported by the success in the development of different prototype machines that showed optimistic results in the production of excellent quality images. In addition, the progress in permanent magnet materials and tridimensional printers has simplified the assembly of powerful multipolar magnets in shorter times.

In this manuscript we briefly review the explored technological approaches for fixed low-field MRI by addressing different critical aspects. Then we introduce the pre-polarized scheme as an advantage within the same context. Finally, the FFC method is proposed as an alternative technique. We show in a simple example how the presence of T_1 dispersive and non-dispersive components in the object to be imaged, conducts to an extremely high contrast. This result is observable by combining pre-polarized and non-polarized field sequences, without the need of any specific contrast agents. Then we focus in the main problems related to this technique: magnetic field inhomogeneity and magnetic field instability. While the first affects the image through geometrical deformation, the second introduces ghosting. We discuss some examples on how both image imperfections can be corrected. Since magnetic field inhomogeneity also affects images acquired with fixed-field instruments based on Halbach magnets, and magnetic field instability is also present in fixed-field electromagnets, the solutions here discussed are also thought for these last cases.

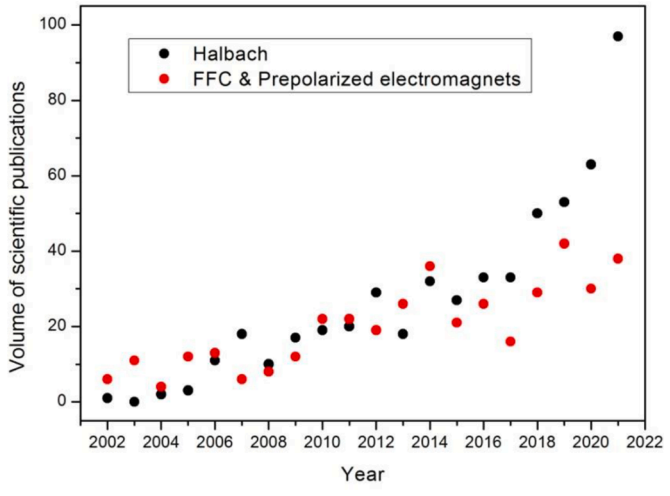

Fig. 1. Evolution of scientific publications associated to Halbach magnets and prepolarized or field-cycling electromagnets (see text for details). A clear increase of publications dealing with Halbach magnets can be observed in the last two years.

2. Low-field MRI technology

In this section we describe some essential features of low-field scanner designs already presented in the literature, address the most typical challenges and the proposed solutions. Then we introduce the concept of pre-polarized MRI.

2.1. Non-cycled low-field scanners

In this subsection, we deal with scanners operating at fixed fields (that is, time independent), including designs based on permanent magnets or electromagnets. Low-field scanners based on permanent magnets are currently the most popular designs. Main advantages of this approach are that neither magnet power supply nor the use of a dedicated cooling system is needed. This fact reduces the involved complexity in the scanner design. However, depending on the magnet material and temperature control system, the main magnetic field could present drifts around 8 ppm/min due to temperature fluctuations [12], or 200 ppm/°C [13].

2.1.1. Multipolar magnets

Several neodymium (NdFeB) magnets mainly based on the Halbach configuration [14] have recently been used for low-field scanners [13, 15–17]. This configuration allows compact and light magnets with relatively small fringe fields. One of the first Halbach configurations used for MRI reported a B_0 of 0.22 T, with a bore of 20 cm and a weight of 50 kg [15]. Prototypes for human brain imaging were reported with a B_0 of 0.05 T and a weight of 75 kg [17], and 0.08 T & 122 kg [16]. Another instrument with 0.072 T & 250 kg was proposed for human extremities [13]. Typical magnetic field inhomogeneities are in the range from 2000 to 3000 ppm within a spherical volume of 28 cm of diameter, which can be used as readout gradient in some cases [16].

2.1.2. Bipolar magnets

Two-pole magnets are also considered for low-field MRI [12,18–20]. This configuration shows better homogeneity although usually heavier than Halbach magnets. In brain scanners [18–20], the B_0 values are between 0.05 T and 0.064 T, with inhomogeneities in the order of 250 ppm within a spherical diameter of 20 cm. Magnets weights are in the range of 350 kg and 750 kg. Samarium-cobalt (SmCo) is often used in bipolar magnets due to its higher stability with temperature [19,20]. In addition, while SmCo is less efficient than the NdFeB in terms of magnetic field intensity, it has a lower temperature remanence coefficient (SmCo 0.015%/°C vs. NdFeB 0.125 %/°C [20–22]).

2.1.3. Other permanent magnets

Single-side brain imaging (although with limited field-of-view) was also considered [23]. This prototype operating at 0.064 T (average field over the imaging region) has a weight (including magnet, gradient unit and RF coil) of 8.3 kg. A 2D imaging system without gradient coils is described in reference [24].

2.1.4. Electromagnets operating at fixed fields

After the pioneering work of Lauterbur [25], Mansfield [26] and others, a whole-body MRI machine was developed in Aberdeen in the late seventies [27]. The instrument was based in a four-coil air-cored electromagnet operating at 0.04 T. In parallel, the development of another instrument was ongoing on at the Central Research Laboratories of Thorn-EMI (Hayes-UK), where a resistive magnet was used to get brain images in 1976. This project evolved with the inclusion of the first commercial cryogenic magnet for MRI (operating at 0.15 T), developed by Oxford Instruments (Oxford-UK) in 1980 (a second magnet was delivered to the University of California, San Francisco – USA) [28]. Therefore, it is worth to observe that first MRI experiments were carried-out with electromagnets, and they have still been successfully used after cryogenic and permanent magnet technologies were adopted

[29–32].

Compared to permanent magnets, electromagnets need a power current supply and, in most cases, a cooling system (at low field, most prototypes operate with air [32]). However, with a proper control system in the power current supply, it is possible to minimize the drifts due to temperature variations. Some exemplary cases can be found in the literature. A B_0 biplane geometry operating at 6.5 mT with an inhomogeneity of 160 ppm was used to imagine several parts of the human body, such as the brain and lung [33,34]. The diameter of the B_0 coils is 2.10 m, and it is inside a Faraday cage [33]. Another instrument using a single-side electromagnet was proposed for neonatal images [31]. It is based on a biplane double-donut design with an operating field of 0.023 T and an inhomogeneity of 600 ppm.

2.2. Challenges and solutions

Challenges in low-field MRI engineering are not only related to the B_0 operating regime, but also with particular constraints derived from the specific applications. We will firstly address limitations originated in the poor SNR, a common issue when dealing with low-field instruments. Then, we will discuss restrictions associated to B_0 inhomogeneity and shielding, which are more challenging in portable scanners.

2.2.1. SNR

A main factor associated with low-field MRI is the loss of SNR with the B_0 field intensity. The SNR is approximately proportional to B_0^x, with an exponent x within the range 1.65–1.7 [35,36]. For example, if x=1.65 the resulting SNR for a 0.05 T scanner is 860 times smaller than the SNR for a 3 T scanner. Two simple solutions to mitigate this disadvantage are i) increase the size of the image pixels (the SNR increases linearly with the pixel volume) and ii) signal averaging (the SNR increases with the square root of the number of averages). These facts explain why the images acquired at low fields usually have lower resolution and longer acquisition times than those obtained in conventional scanners operating at 1.5 T or 3 T. However, these simple solutions attempt against the image quality and usefulness of the approach. These undesirable consequences have inspired several acquisition and post-processing methods developed to increase the resolution [37,38] and minimize the acquisition times [39,40].

A clear advantage of low-field instruments relies in the possibility of using more complex pulse sequences. As the specific absorption rate (SAR) is proportional to B_0^2, radio-frequency (RF) power deposition in the sample is much lower at low-fields. In fact, it is possible to implement pulse sequences with flip angles of 180° to maximize the signal refocusing. For example, 3D balanced steady-state free precession sequences can be used to maximize the SNR per unit of time [34,40–42]. Another factor that plays in favor is the fact that T_1 contrast between certain tissues tends to increase at low fields. For example, the maximum contrast between white and gray matter occurs at 0.25 T [43]. Worth to mention is the fact that specific contrast agents based on super-paramagnetic iron oxide nanoparticles [44–46] or hyperpolarization [33,47,48] can substantially increase the low-field sensitivity.

2.2.2. B_0 inhomogeneity

B_0 inhomogeneity depends on the magnet geometry. Halbach magnets show values usually>2000 ppm [13,16,17]. The main consequence of B_0 inhomogeneity is a position-dependent spin dephasing, thus provoking image distortion. Dephasing by static magnetic field inhomogeneity is a reversible phenomenon, and consequently it can be compensated using adequate pulse sequences and data post-processing. Fast spin-echo or rapid imaging with refocusing echo (RARE) [49] sequences [13,16,17] are commonly used in this context. Despite the fact that spin-echo sequences are less affected by the inhomogeneity than gradient-echo sequences, the images still show distortions that need to be corrected. Recently, two post-processing methods were proposed to minimize distortions in images acquired under high inhomogeneities [50,51]. These methods proposed the acquisition of two images from which the inhomogeneity map can be calculated, and then use this information for correction.

2.2.3. Shielding

A main problem for portable scanners relies in the fact that the human body operates as an antenna, a tricky situation if the instrument is operating in the absence of a shielded room. One of the most popular strategies is the use of metallic clothes as passive shielding [12,13,17]. However, while this approach showed good results, it can be quite uncomfortable for the patient. Other strategies use pick-up coils and sensors that monitors the noise during the image acquisition, and later use this information to remove noise from the images [20,52].

2.3. Pre-polarized MRI

In this approach, a higher magnetic field B_P is used to boost-up the magnetization, and then the system is settled to a lower field B_A where the MRI sequence and signal acquisition is performed [3–6]. The polarization field is usually of the order of 0.5 T (or lower). The fact that B_P>B_A increases the final SNR if compared to an experiment performed at a fixed field B_A. In particular, if the polarization-field pulse is applied long enough to saturate the magnetization, the SNR can be expressed as [53]:

$$SNR \approx B_P \varepsilon \sqrt{\frac{\sigma Q V_S \omega_A}{K_B T \Delta\omega}}. \quad (1)$$

In this equation ε represents the reciprocal noise level of the receiver, σ the filling factor, Q is the quality factor of the coil, V_s the sample volume, K_B the Boltzman constant, T the temperature, $\omega_A = \gamma B_A$ (Larmor frequency at which the signal acquisition is performed), and $\Delta\omega$ the receiver bandwidth. As ω_A is proportional to B_A, we can conclude that the SNR is approximately linear with B_P, and proportional to the square root of B_A [8,54]. Therefore, while for a pre-polarized scanner with B_P = 0.5 T and B_A = 0.05 T the SNR should be approximately 86 times smaller than for a 3 T scanner, it would still represent an increment of 10 times compared with the SNR of a fixed-field scanner operating at 0.05 T. That is, pre-polarizing decreases the losses of SNR while keeping the advantage of detecting at low field (low SAR, favorable relaxometry properties, high sensitivity and low susceptibility).

Pre-polarized systems usually have two different magnets, one to generate B_P and the other magnet for B_A. Usually, an electromagnet is used to generate the polarization field and another magnet, either permanent, resistive, or even the earth magnetic field, for the acquisition [6,8]. A pre-polarized scanner using a combination of two permanent magnets, settled in a rotary arrangement to change between polarization and acquisition modes is described in [55]. The fact that two different magnets are normally used makes pre-polarized systems more complex. In addition, to reach polarization fields higher than 0.1 T with electromagnets, it is necessary to implement cooling systems based on water or other fluids [4,6,8], thus hindering their portability. Nonetheless, as the requirements for homogeneity and stability for generators of polarizing field are minimal, their construction is greatly simplified.

3. Fast field-cycling MRI

From the previous sections, we may conclude that low-field technology represents an important opportunity to introduce low-cost MRI-based diagnosis in the health system. However, we had also remarked some intrinsic difficulties, like images acquired with higher noise level, and with severe geometrical distortions due to magnetic field inhomogeneity. The use of magnetic fields with higher intensity and homogeneity may compensate such limitations but at an increased cost [56,57]. In addition, the use of higher magnetic fields severely affects the portability and introduces a more complex risk management [58].

The suboptimal T_1 contrast can be conveniently skipped by cycling the magnetic field between different values. This practice allows the spin-system to evolve at lower magnetic field intensities of the order (or lower) than 0.01 T. In contrast with the pre-polarized version as presented in Section 2.3., here we may switch-up the magnetic field to a convenient value were signal acquisition can be performed after a period during which, the spin system has evolved or been manipulated using proper physical interactions, or under the action of specific chemicals.

The suboptimal T_1 contrast at fixed-field MRI can be conveniently replaced by T_1 relaxation dispersion contrast, a possibility that is only available within a field-cycled scheme. Fig. 2 shows how T_1 at a Larmor frequency of 2 MHz may be quite insensitive to discriminate different tissues, while a contrast parameter based on T_1 dispersion can show a better performance. In this case ΔT_1 is defined as T_1(10 MHz) – T_1(10 kHz).

Cycling of the magnetic field is a well-known ruse to perform NMR experiments at field intensities where spin polarization would be negligible at fixed-field conditions. In the last years, the field-cycling technology has evolved from simple T_1 (or $R_1 = 1/T_1$) relaxometry experiments (relaxation dispersion curves) in a variety of samples [54,60–64], to more sophisticated experiments involving double-resonances with quadrupolar nuclei or electrons [36,65,66], FFC-MRI [3,7–10,67] or FFC-MRI relaxometry [45,68–70]. Fig. 3 shows a pre-polarized and non-polarized pulse sequences recently used for FFC-MRI. Usually, the detection field is the same for both sequences. This maximizes the SNR while operating at a fixed RF frequency.

FFC experiments require a fast switching of the magnetic field. The use of a single air-cored electromagnet is commonly considered for the design of these instruments [54,70,71–76]. The electromagnet is fed by a current source, which defines the time-stability of the magnetic field. Here, the image acquisition may be severely distorted due to both the magnetic field inhomogeneity and its short-term instability [10,51,68,69,73]. Systems combining different magnet technologies are not affected by short-term instability, as far as the electromagnet is only used for pre-polarizing the spin-system. Iron-based electromagnets can also be considered for field-cycled applications [70]. Magnets cored with high magnetic permeability materials allows strongly reducing the needed current for a given magnetic field intensity [77]. In these cases, the power reduction may be important.

Field-cycling allows to image samples that may evolve at different magnetic field values. This fact represent an important technical advantage that is absent in fixed-field scanners. Fig. 4 shows an example of images acquired with a FFC-MRI relaxometer at different field intensities. The sample consists of two horizontal tubes filled with an aqueous solution (AS) of deionized water with copper sulfate and two vertical tubes of Polydimethylsiloxane (PDMS). The graph in the bottom middle of the figure shows the dispersive curves of both compounds. The image A was acquired at a low relaxation field with a pre-polarized sequence. Under these conditions, the PDMS component relaxes completely during the relaxation field, resulting in an image where only the signal contribution comes from the AS. The image C of the figure was acquired with a non-polarized sequence, at a relaxation field where both components have the same T_1. Therefore, the image C is weighted mainly by proton density. Finally, the image B is the difference between the images C and A, resulting in an image with principal signal contribution from the PDMS.

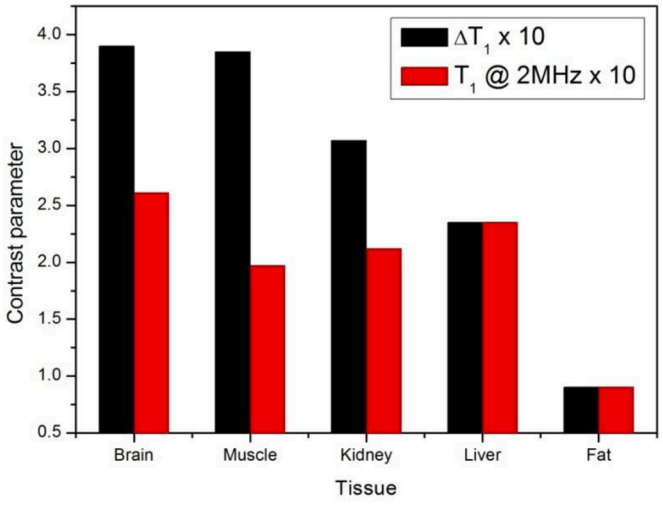

Fig. 2. Differences between T_1 measured at a Larmor frequency of 2 MHz and ΔT_1 calculated as the difference in T_1 between 10 MHz and 10 kHz (murine tissue). In the plot both parameters are scaled by a factor 10. Original data acknowledged to the authors of reference [59].

As another example of the opportunities that field-cycling offers, we may mention the possibility to profit the nuclear-quadrupole interaction as a potential source of contrast or even as a biomarker [67,79–81]. Similar situations are feasible using other interactions, double resonances or exploiting the possibility to manipulate the spin-system a low or zero-field [7,68,70,82,83]. All this background offers still unexplored possibilities for the design of new biomarkers and contrast agents that are not feasible in a fixed-field scheme.

The academic growing interest in the field is represented in Fig. 5. The figure shows 3 curves representing the growing interest of: low-field MRI (permanent magnets), portable MRI and both FFC & prepolarized. Data were collected using Scholar Google and searching by trienniums the total number of published papers under the strings ("low-field MRI" AND "permanent magnet"), "portable MRI" and ("FFC MRI" OR "Pre-polarized MRI"). Results show that until 2012 all the tendencies were similar. However, in the last years, the interest in permanent magnet solutions increased. Some of these include pre-polarized technology. Noteworthy, portability started to be a trending topic in 2016, showing an increased activity in the last triennium.

4. Challenges and opportunities for the field-cycled technology

Low-field & low-cost scanners will not replace the standard MRI infrastructure used today at important health centers. However, locations that are far away from such main centers, may access to a basic or preliminary diagnosis using low-cost instrumentation. Even in heath centers located in big cities, low-cost instrumentation can be used to routinely screening or certain cases that do not justifies the use of a high-field superconducting magnet scanner. In addition, portability is welcomed if the instrument can be moved on wheels, or even fixed in an adequate transportation.

From these speculative assumptions, we may potentially identify four different categories of low-field instruments:

I Non-cryogenic, but devised for a fixed installation in a dedicated room. Weight & size are not a limiting factor.
II Compact & benchtop approach. Easy to reinstall, but not portable. Weight and size starts to be a limiting factor.
III Intended for operative conditions installed on a vehicle for transportation. Weight, size and power management are important points.
IV Compact & fully portable. Light and easy to move. Weight, size and power management are critic.

In the current state of the art, field cycled solutions can be realistically considered for cases I and II, and with a moderate engineering effort, even for case III. The evolution of electromagnet technology, power electronics and batteries, will surely allow solutions for case IV in a short time.

In this section we will discuss in more detail relevant aspects to confront when dealing with electromagnet-based field-cycling instruments.

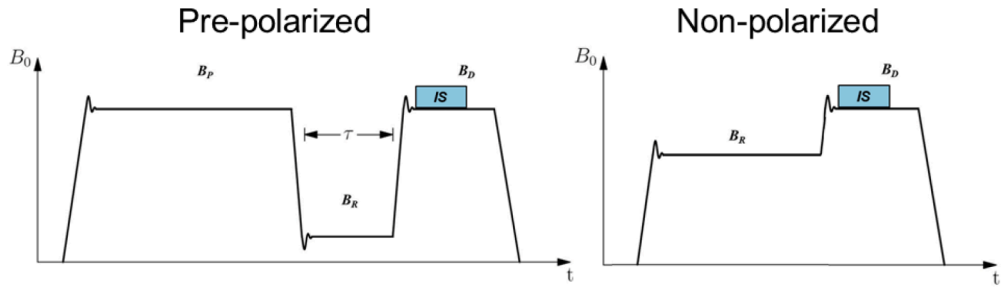

Fig. 3. FFC-MRI pulse sequences. B_P: polarizing field. B_R: relaxation field. B_D: detection field. τ: evolution time. The IS rectangle represents the image acquisition sequence. In the NP sequence, no polarization field is applied.

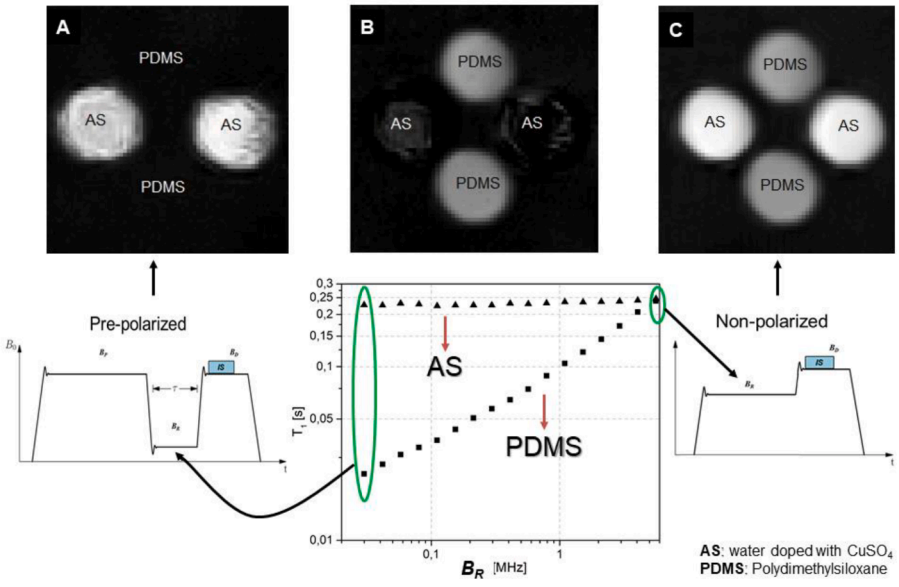

Fig. 4. Images acquired at different field intensities with a FFC-MRI relaxometer. Bottom left: pre-polarized sequence used for acquiring image A. At a low field, the PDMS component relaxes completely, resulting in a contrast close to 100%. Bottom middle: dispersion curves of aqueous solution AS (triangles) and PDMS (squares) [78]. Bottom right: non-polarized sequence used for acquiring image C, at this field, both samples have the same T1 resulting in an image mainly weighted by proton density. Image B is the difference between the images C and B.

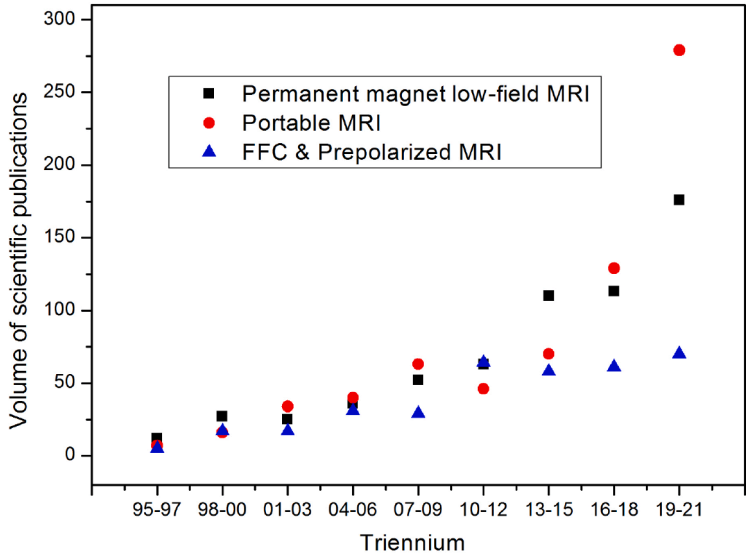

Fig. 5. Tendencies of the volume of scientific publications dealing with low-field (permanent magnet), portable and prepolarized & field-cycled MRI. A strong increase in the interest for portable machines can be observed in the last triennium.

4.1. Field-cycling MRI under high B_0 magnetic field inhomogeneity

We will briefly refer to some features related to image acquisition under high magnetic field inhomogeneities (>1000 ppm). We will also discuss some strategies to minimize image artifacts. The experiments here presented were performed in an MRI relaxometer of own design,

operating with a magnetic field inhomogeneity of 1400 ppm within a cylindrical volume of 35 mL [69]. This inhomogeneity is a bit lower to those of multipolar fixed-field magnets, which are the configurations with higher inhomogeneity among the different low-field designs (see Section 2.1.1). The magnet used in the experiments to be shown, can also be configured to have 300 ppm field homogeneity [76].

Since images were acquired under high B_0-inhomogeneity conditions, the spin-echo sequence was adopted [84]. The image sequence is synchronized in two different field-cycling schemes: pre-polarized (PP) and non-polarized (NP), see Fig. 3.

4.1.1. Magnetic field characterization and slice orientation

The knowledge of the principal direction of the magnetic field inhomogeneity can be used to minimize the image degradation. A simple way to determine the principal direction of the inhomogeneity is to measure the full width half maximum (FWHM) of the Fourier transform of the signals acquired from a plane around different orientation [78]. Fig. 6 1) shows the results obtained by rotating a rectangular planar sample (40 × 28 × 2 mm^3) along the z-axis direction (B_0 direction). These results suggest that the main inhomogeneity has a principal direction in the transverse plane (*x*-*y*). Then, it is convenient to redefine the coordinate system aligning *x* with the principal inhomogeneity direction.

Once the principal direction of the inhomogeneity is known, the distortions in 2D images can be reduced in the following ways:

- Acquiring 2D images in a plane perpendicular to the principal inhomogeneity direction (plane *y*-*z*).
- If images need to be acquired in the *x*-*y* or *x*-*z* plane, aligning the read gradient along the *x* direction.

The first case minimizes the inhomogeneity within the image plane, while the second case takes advantage of the inhomogeneity, using its linear component as part of the encoding gradient. Fig. 6 2A shows an image acquired in the *x*-*z* plane, with the read gradient along the *z* direction, and 2C shows an image acquired in the *y*-*z* plane with the read gradient applied in the *z* direction. Both were acquired using the previously mentioned rectangular phantom. Figures B and D correspond to transverse images acquired after changing the sample for a cylindrical container. 2B corresponds to an image acquired in the *x*-*y* plane, with the read gradient applied along the*y* direction, while 2D shows an image acquired in the *x*-*y* plane with the read gradient applied in the *z* direction.

4.1.2. Polarity inversion of the readout gradient

Image distortions due to high magnetic field inhomogeneity can be corrected after acquiring two different images under slightly different conditions (as far as the magnetic field inhomogeneity is time independent) [50,51]. We show the results obtained by acquiring two images, one of them after reversing the readout gradient [69]. Fig. 7 shows the images acquired with a phantom of three columns filled with different heights of water (doped with copper sulfate). The image i_1 was acquired with the read gradient in opposite direction than the inhomogeneity; hence, the effective gradient is smaller. i_2 was acquired with the read gradient in the same direction than the inhomogeneity, resulting in a higher effective gradient. Finally, the image *i* is the corrected image using i_1 and i_2. The method can also be used to estimate the magnetic field map, thus allowing new corrections without needing the acquisition of two images for every scan session. It should be noted that this statement is valid as far the magnetic field homogeneity is nearly the same for each scan. This can be a minor problem in fixed-field thermostatted arrays of permanent magnets. However, in some FFC magnets, the thermomechanical stress changes as the magnet heats-up during a current pulse, a topic to keep in mind when considering the cooling hydrodynamics and the thermal dissipation properties across the magnet. An excess of thermomechanical stress may modify the magnet geometry, and consequently, the magnetic field homogeneity map.

4.1.3. SNR dependence on the magnet inhomogeneity

So far, we have mentioned different strategies to minimize image artifacts generated by the inhomogeneity of the B_0 field. However, image distortion is not the unique undesirable consequence for MRI caused by magnetic field inhomogeneity. In fact, the dephasing produced by the inhomogeneity provokes signal losses that affect the total SNR. Therefore, higher inhomogeneities will demand a higher number of signal acquisitions to compensate for these losses, thus increasing the total scan time.

Fig. 8 shows images acquired under different inhomogeneities with their respective SNR. The three images were acquired with the exact same parameters. 760 ppm was obtained by applying a first order shim (compensating the linear component of the inhomogeneity). 2600 ppm was obtained by moving the sample outside of the center of the magnet. As expected, the SNR decrease with the inhomogeneity. In addition, image distortion is homogeneity-dependent (the magnetic field distribution is different for each case).

4.2. Field-cycling MRI under high B_0 magnetic field instability

Magnetic field instabilities represent one of the main challenges for

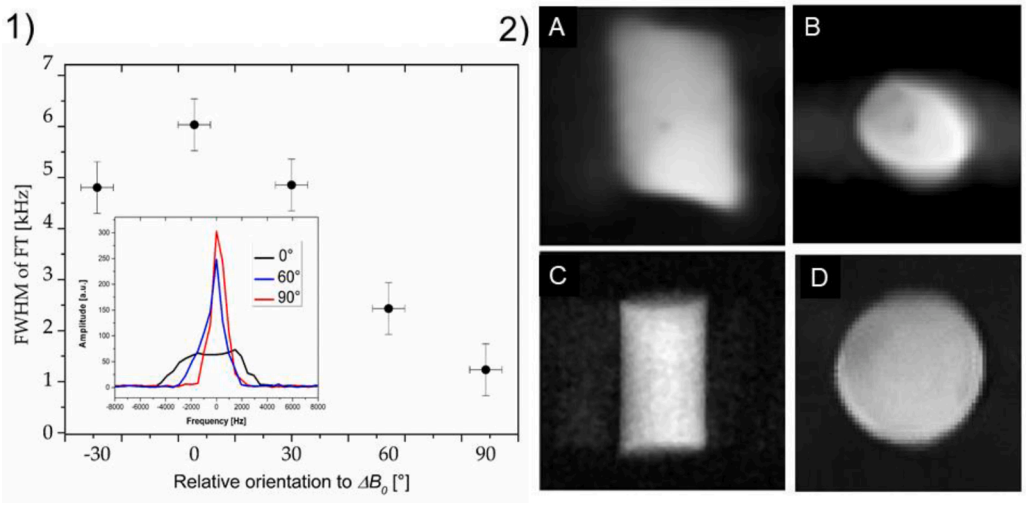

Fig. 6. 1) Full width of half maximum (FWHM) of Fourier transform for signals acquired from different orientations of the planar sample. The inset shows the strong difference in the FWHM by rotating the sample 90°. 2) 2D images acquired along different orientations. A and C were obtained using a rectangular phantom while B and D correspond to a cylindrical tube (see text for details). All images are 64 × 64 pixels and 1024 μs readout time. For sagittal images G_p = (11.9 ± 0.1)mT/m, ET = 2 ms, 4 scans. For transversal images G_P = (190.1 ± 0.1)mT/m, ET = 1 ms, 2 scans. G_R gradient values are: G_R = (31.5 ± 0.1) mT/m for A, G_R = (60.4 ± 0.1)mT/m for B, G_R = (42.0 ± 0.1)mT/m for C and G_R = (82.4 ± 0.1)mT/m for D. Here G_p and G_R stands for phase and readout gradients and *ET* for echo time.

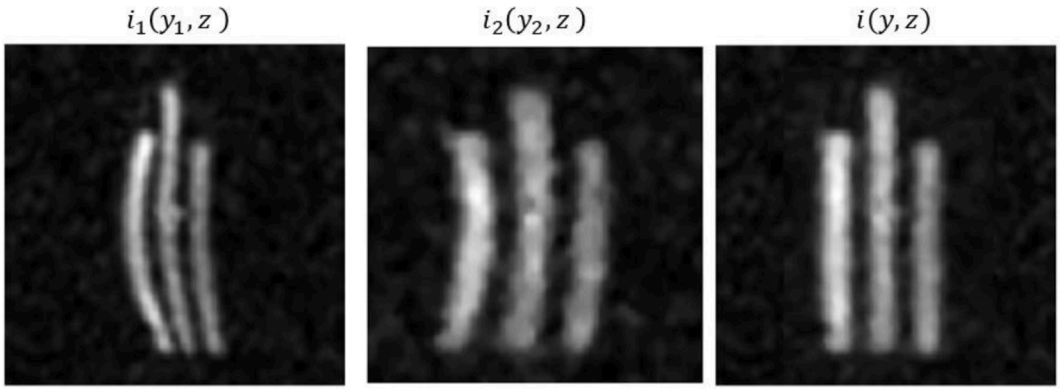

Fig. 7. Images obtained by inverting the polarity of the read gradient (i_1 and i_2), and the corrected image i (see text for details). Image i_1 was acquired with the read gradient oriented in the opposite direction of the inhomogeneity. Image i_2 was acquired with the read gradient in the same direction than the inhomogeneity. $G_R = \pm(21.3 \pm 0.1)$mT/m, $G_p = (21.0 \pm 0.1)$mT/m, ET = 2 ms, readout time = 1024 μs, 16 scans, matrix size:64 × 64 pixels (resized to 256 × 256).

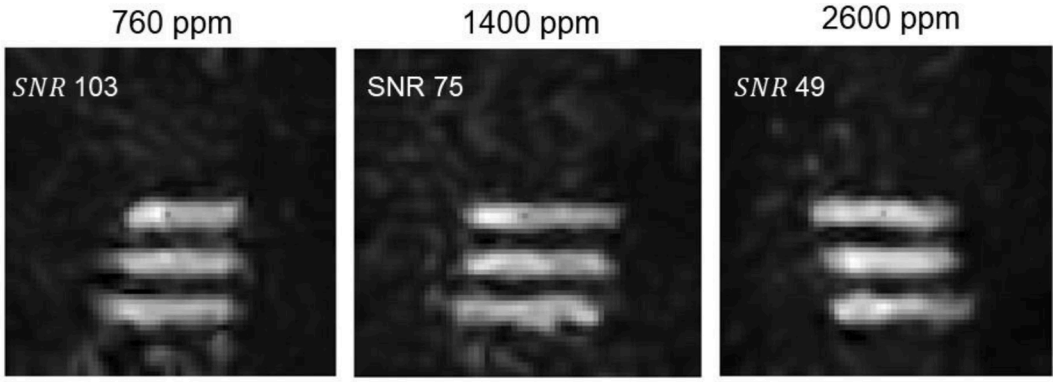

Fig. 8. Images acquired under different magnetic field inhomogeneities. All the images were acquired with the same parameters. $G_R = (60.4 \pm 0.1)$mT/m, $G_p = (73.5 \pm 0.1)$mT/m, ET = 1 ms, readout time = 1024 μs, 8 scans, matrix size:64 × 64 pixels.

FFC-MRI. As B_0 is usually generated through an electromagnet, the instabilities are higher than in scanners based on other techniques; with values that can reach hundreds of ppm between acquisitions [52,69,84]. Moreover, a main issue in these kinds of instruments is associated with the current power supply and its control system, in order to allow for fast switching with short transients and stable acquisition fields [68]. Fortunately, with the computing power available today at a low cost, instability-induced image ghosting can be practically eliminated with adequate post-processing algorithms in times that are compatible with experimental cycles. Worth to mention, this is a critical point towards low-cost & field-cycled instrumentation.

4.2.1. *Instability artifact corrections*

The magnetic field instability provokes phase accumulations generating image artifacts (usually manifested as ghosting) along the phase direction. Currently, there are two main strategies to mitigate this undesirable effect. The first one consists in reducing the echo time (ET) in the pulse sequence, minimizing the undesired accumulated phase [67]. The second one consists in applying post-processing methods to correct the image artifacts along the phase direction [51,85]. Both strategies are complementary and can be implemented simultaneously. However, depending on the instability characteristics, hardware limitations, and the desired contrast, the reduction of the ET may not be the optimal solution.

In the following, we compare both strategies as tested in our FFC-MRI relaxometer [69]. The magnetic field instability was settled to 220 ppm between acquisitions. The instability was determined from the standard deviation of the frequency shifts of the acquired NMR signals. The peak value of the Fourier transform (FT) of the echo was measured over 50 signal samples. All the images were acquired with a spin-echo sequence and Cartesian acquisition. Fig. 9 shows the images acquired with an ET = 2 ms and ET = 5 ms, and the image with ET = 5 ms after post-processing correction using the method described in reference [51]. The image with ET = 2 ms do not show artifacts associated with the instability, while the image acquired with ET = 5 ms shows several artifacts along the phase direction (y). After correction, the image corresponding to ET = 5 ms recovers practically the same quality of that corresponding to ET = 2 ms. Fig. 10 shows an image acquired with ET = 2 ms and its corrected version. In this particular case, the echo time of 2 ms was not enough to acquire an image without artifacts. However, the post-processing method corrects most of the generated artifacts.

Images shown in Figs. 9 and 10 are also distorted by magnetic field inhomogeneity. However, in this subsection we have only focused on ghosting cancellation due to magnetic field instability.

5. Summary and concluding remarks

In this manuscript we have briefly analyzed the state of the art of low-field MRI. A clear increasing interest in the field can be deduced from the literature, patents and ongoing activity at industrial environment. The existence of one product in the market, and several industrial developments in progress, portends an optimistic panorama in a near future. The involved engineering has an advanced degree of maturity today, providing a fertile terrain for a fast growing of this, although not new, but revived branch of MRI. Our analysis indicates a clear tendency towards portability and low-cost instrumentation.

Field-cycled solutions have already showed excellent performance in pre-polarized schemes. Although not yet explored, excepted category I

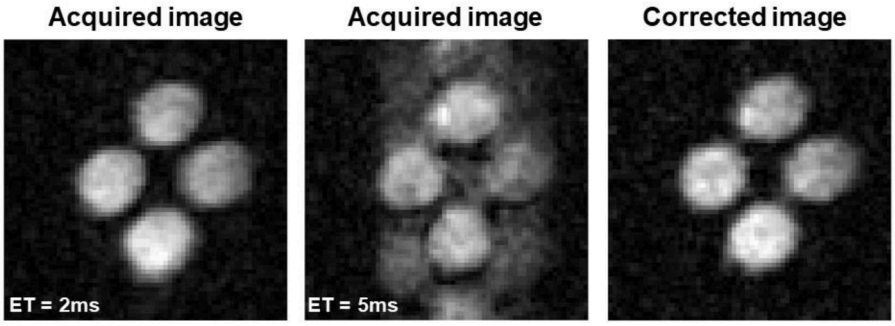

Fig. 9. Images under high magnetic field instability. Left: image acquired with an echo time of 2 ms. Center: image acquired with an echo time of 5 ms. Right: the result of the center image after post-processing instability corrections. $G_R = (54.9 \pm 0.1)$mT/m, $G_p = (106.9 \pm 0.1)$mT/m, readout = 1024 μs, 2 scans, matrix size:64 × 64 pixels.

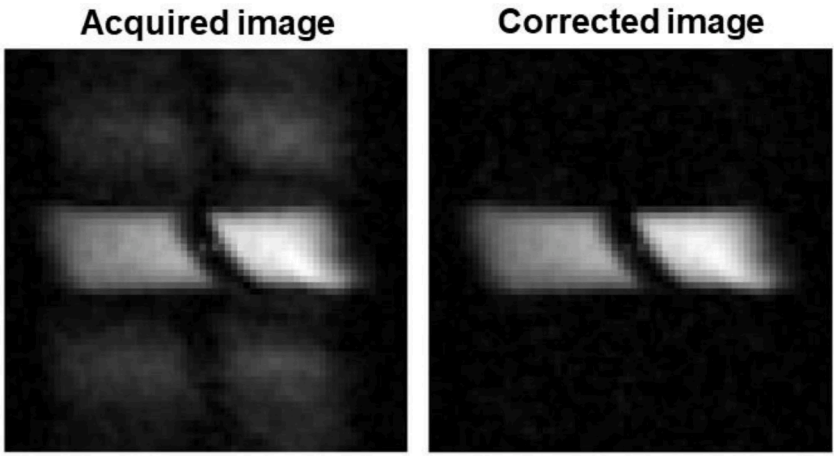

Fig. 10. Images under high magnetic field instability (220 ppm). Left: image acquired with an echo time of 2 ms. Right: the result of the center image after post-processing instability corrections. $G_R = (54.9 \pm 0.1)$mT/m, $G_p = (106.9 \pm 0.1)$mT/m, readout = 1024 μs, 2 scans, matrix size:64 × 64 pixels.

(Section 4), FFC-MRI may also derive in solutions defined in the other categories. Perhaps, from a conservative point of view, the future of portable FFC-MRI scanners remains as an open possibility. In any case, several technological advances associated to FFC-MRI will surely be of advantage for pre-polarized instruments. In view of the post-processing capabilities that are feasible today at a low/moderate cost, a return to electromagnet technology as a unique magnetic field source in pre-polarized schemes may turn into an interesting possibility. However, a main challenge in this direction pertains to the success in using low-cost & low-weight switched-mode power supplies (SMPS), in combination with the inclusion of high magnetic susceptibility materials and efficient cooling systems. A key feature for the success of the FFC technology for MRI-based diagnosis remains in a variety of field-dependent experiments that can be implemented for the design of specific contrasts and biomarkers, a possibility that is more limited for fixed-field instruments.

In the context of portability, definitely the use of magnets with poor homogeneity represents a key-way for reducing costs. B_0 magnet gradients can be used for encoding, while image distortions can be mitigated with hardware ruses and mathematical manipulation. If electromagnets are to be entering into play, we have shown that even high current stability is not needed, since ghosting can be practically eliminated with adequate algorithms. In this context, our FFC-MRI relaxometer is an excellent tool for the investigation of all these limiting situations.

Declaration of Competing Interest

The authors declare that they have no known competing financial interests or personal relationships that could have appeared to influence the work reported in this paper.

Data availability

Data will be made available on request.

Acknowledgements

The authors acknowledge financial support from FONCYT PICT 2017-2195, CONICET 11220200102521CO and Secyt UNC PRIMAR 34020190100004CB, Argentina. The authors also acknowledges original data used to produce Fig. 2 to the authors of reference 59 (Araya, Martínez-Santisteban, Handler, Harris, Chronik and Scholl).

References

[1] D.I. Hoult, S. Goldstein, J. Caponiti, Electromagnet for nuclear magnetic resonance imaging, Rev. Sci. Instrum. 52 (1981) 1342–1351.
[2] K.N. Sheth, M.H. Mazurek, M.M. Yuen, B.A. Cahn, et al., Assessment of brain injury using portable, low-field magnetic resonance imaging at the bedside of critically ill patients, JAMA Neurol 78 (2021) 41–47.
[3] -E. Yamamoto, S. Kensuke, K. Ideki, Nuclear magnetic resonance device, Japan Patent JPS57211539 (A) (1982).
[4] P. Morgan, S. Conolly, G. Scott, A. Macovsky, A readout magnet for prepolarized MRI, Magn. Reson. Med 36 (1996) 527–536.
[5] R.D. Venook, N.I. Matter, M. Ramachandran, S.E. Ungersma, et al., Prepolarized magnetic resonance imaging around metal orthopedic implants, Magn. Reson. Med. 56 (2006) 177–186.
[6] J. Borreguero Morata, J.M. González, E. Pallás, J.P. Rigla, et al., Prepolarized MRI of hard tissues and solid-state matter, NMR Biomed 35 (2022), 4737.

[7] D.J. Lurie, J.M.S. Hutchinson, L.H. Bell, I. Nicholson, D.M. Bussell, J.R. Mallard, Field-cycled proton-electron double-resonance imaging of free radicals in large aqueous samples, J. Magn. Reson. 84 (1989) 431–437.

[8] N.I. Matter, G.C. Scott, T. Grafendorfer, A. Macovski, S.M. Conolly, Rapid polarizing field cycling in magnetic resonance imaging, IEEE Trans. Med. Imag. 25 (2006) 84–93.

[9] K.M. Gilbert, W.B. Handler, T.J. Scholl, J.W. Odegaard, B.A. Chronik, Design of field-cycled magnetic resonance systems for small animal imaging, Phys. Med. Biol. 51 (2006) 2825–2841.

[10] L.M. Broche, P.J. Ross, G.R. Davies, M.-J. McLeod, D.J. Lurie, A whole-body fast field-cycling scanner for clinical molecular imaging studies, Sci. Rep. 9 (2019), https://doi.org/10.1038/s41598-019-46648-0.

[11] M. Bödenler, O. Maier, R. Stollberger, L.M. Broche, et al., Joint multi-field T_1quantification for fast field-cycling MRI, Magn. Reson. Med. 86 (2021) 2049–2063.

[12] M. Nakagomi, M. Kajiwara, J. Matsuzaki, K. Tanabe, et al., Development of a small car-mounted magnetic resonance imaging system for human elbows using a 0.2T permanent magnet, J. Magn. Reson. 304 (2019) 1–6.

[13] T. Guallart-Naval, J.M. Algarín, R. Pellicer-Guridi, F. Galve, et al., Portable magnetic resonance imaging of patients indoors, outdoors and at home, Sci. Rep. 12 (2022), 13147.

[14] K. Halbach, Design of permanent multipole magnets with oriented rare earth cobalt material, Nucl. Instrum. Methods. 169 (1980) 1–10.

[15] E. Danieli, J. Mauler, J. Perlo, B. Blumich, F. Casanova, Mobile sensor for high resolution NMR spectroscopy and imaging, J. Magn. Reson. 198 (2009) 80–87.

[16] C.Z. Cooley, P.C. McDaniel, J.P. Stockmann, S. Abitha Srinivas, et al., A portable scanner for magnetic resonance imaging of the brain, Nat. Biomed. Eng. 5 (2021) 229–239.

[17] T. O'Reilly, W.M. Teeuwisse, D. de Gans, K. Koolstra, et al., In vivo 3D brain and extremity MRI at 50 mT using a permanent magnet Halbach array, Magn. Reson. Med. 85 (2021) 495–505.

[18] S.C.L. Deoni, P. Medeiros, A.T. Deoni, P. Burton, et al., Development of a mobile low-field MRI scanner, Sci. Rep. 12 (2022), 5690.

[19] Y. He, W. He, L. Tan, F. Chen, et al., Use of 2.1 MHz MRI scanner for brain imaging and its preliminary results in stroke, J. Magn. Reson. 319 (2020), 106829.

[20] Y. Liu, A.T.L. Leong, Y. Zhao, L. Xiao, et al., A low-cost and shielding-free ultra-low-field brain MRI scanner, Nat. Commun. 12 (2021), 7238.

[21] M. Sagawa, S. Fujimura, N. Togawa, H. Yamamoto, et al., New material for permanent magnets on a base of Nd and Fe, J. Appl. Phys. 55 (1984) 2083–2087.

[22] P. Campbell, Permanent Magnet Materials and their Application, Cambridge University Press, Cambridge, 1994, pp. 57–81.

[23] P.C. McDaniel, C.Z. Cooley, J.P. Stockmann, L.L. Wald, The MR cap: a single-sided MRI system designed for potential point-of-care limited field-of-view brain imaging, Magn. Reson. Med. 82 (2019) 1946–1960.

[24] C.Z. Cooley, J.P. Stockmann, B.D. Armstrong, M. Sarracanie, et al., Two-dimensional imaging in a lightweight portable MRI scanner without gradient coils, Magn. Reson. Med. 73 (2015) 872–883.

[25] P.C. Lauterbur, Image formation by induced local interactions: examples employing nuclear magnetic resonance, Nature 242 (1973) 190–191.

[26] A.N. Garroway, P.K. Grannell, P. Mansfield, Image formation in NMR by a selective irradiative process, J. Phys. C.: Solid State Phys. 7 (1974) L457–L462.

[27] W.A. Edelstein, J.M.S. Hutchison, F.W. Smith, J. Mallard, et al., Human whole-body NMR tomographic imaging: normal sections, Br. J. Radiol. 54 (1981) 149–151.

[28] F.H. Doyle, I.R. Young, J.M. Pennock, H. Clow, et al., Imaging of the brain by nuclear magnetic resonance, Lancet 318 (1981) 53–57.

[29] S.K. Mun, I.K. Mun, Cryogenics in superconducting magnets for MRI, J. Radiol. Eng. 4 (1986) 7–11.

[30] P.N. Morgan, S.M. Conolly, A. Macovski, Resistive homogeneous MRI magnet design by matrix subset selection, Magn. Reson. Med. 41 (1999) 1221–1229.

[31] S. Lother, S.J. Schiff, T. Neuberger, P.M. Jakob, et al., Design of a mobile, homogeneous, and efficient electromagnet with a large field of view for neonatal low-field MRI, Magn. Reson. Mater. Phy. 29 (2016) 691–698.

[32] F. Natukunda, T.M. Twongyrwe, S.J. Schiff, J. Obungoloch, Approaches in cooling of resistive coilbased low-field magnetic resonance imaging (MRI) systems for application in low resource settings, BMC Biomed. Eng. (2021), https://doi.org/10.1186/s42490-021-00048-6 doi.org/.

[33] L.L. Tsai, R.W. Mair, M.S. Rosen, S. Patz, R.L. Walsworth, An open-access, very-low-field MRI system for posture-dependent 3He human lung imaging, J. Magn. Reson. 193 (2008) 274–285.

[34] M. Sarracanie, C.D. LaPierre, N. Salameh, D.E.J. Waddington, et al., Low-cost high-performance MRI, Sci. Rep. 5 (2015), 15177.

[35] D.I. Hoult, R. Richards, The signal-to-noise ratio of the nuclear magnetic resonance experiment, J. Magn. Reson. 24 (1976) 71–85.

[36] R. Pohmann, O. Speck, K. Scheffler, Signal-to-noise ratio and MR tissue parameters in human brain imaging at 3, 7, and 9.4 tesla using current receive coil arrays, Magn. Reson. Med. 75 (2016) 801–809.

[37] J.E. Iglesias, B. Billot, Y. Balbastre, A. Tabari, et al., Joint super-resolution and synthesis of 1 mm isotropic MP-RAGE volumes from clinical MRI exams with scans of different orientation, resolution and contrast, Neuroimag 237 (2021), 118206.

[38] M.L. de Leeuw den Bouter, G. Ippolito, T. O'Reilly, R.F. Remis, et al., Deep learning-based single image super-resolution for low-field MR brain images, Sci. Rep. 12 (2022), 6362.

[39] N. Koonjoo, B. Zhu, G.Cody Bagnall, D. Bhutto, et al., Boosting the signal-to-noise of low-field MRI with deep learning image reconstruction, Sci. Rep. 11 (2021), 8248.

[40] R. Ayde, T. Senft, N. Salameh, M. Sarracanie, et al., Deep learning for fast low-field MRI acquisitions, Sci. Rep. 12 (2022), 11394.

[41] K. Scheffler, S. Lehnhardt, Principles and applications of balanced SSFP techniques, Eur. Radiol. 13 (2003) 2409–2418.

[42] A. Oppelt, R. Graumann, H. Barfuss, H. Fischer, et al., FISP—a new fast MRI sequence, Electromed. 54 (1986) 15–18.

[43] H.W. Fischer, P.A. Rinck, Y. Van Haverbeke, R.N. Muller, Nuclear relaxation of human brain gray and white matter: analysis of field dependence and implications for MRI, Magn. Reson. Med. 16 (1990) 317–334.

[44] X. Yin, S.E. Russek, G. Zabow, F. Sun, et al., Large T1 contrast enhancement using superparamagnetic nanoparticles in ultra-low field MRI, Sci. Rep. 8 (2018), 11863.

[45] G.G. Rodriguez, E.M. Erro, E. Anoardo, Fast iron oxide-induced low-field magnetic resonance imaging, J. Phys. D: Appl. Phys. 54 (2020), 2.

[46] D.E. Waddington, T. Boele, R. Maschmeyer, Z. Kuncic, et al., High-sensitivity in vivo contrast for ultra-low field magnetic resonance imaging using superparamagnetic iron oxide nanoparticles, Sci. Adv. 6 (2020), 998.

[47] A.M. Coffey, M.L. Truong, E.Y. Chekmenev, Low-field MRI can be more sensitive than high-field MRI, J. Magn. Reson. 237 (2013) 169–174.

[48] K.V. Kovtunov, M.L. Truong, D.A. Barskiy, I.V. Koptyug, et al., Long-lived spin states for low-field hyperpolarized gas MRI, Chem. Eur. J. 20 (2014) 14629–14632.

[49] J. Hennig, A. Nauerth, H. Friedburg, RARE imaging: a fast imaging method for clinical MR, Magn. Reson. Med. 3 (1986) 823–833.

[50] K. Koolstra, T. O'Reilly, P. Börnert, A. Webb, Image distortion correction for MRI in low field permanent magnet systems with strong B0 inhomogeneity and gradient field nonlinearities, MAGMA 34 (2021) 631–642.

[51] G.G. Rodriguez, A. Salvatori, E. Anoardo, Dual k-space and image-space post-processing for field-cycling MRI under low magnetic field stability and homogeneity conditions, Magn. Reson. Imaging 87 (2022) 157–168.

[52] S.A. Srinivas, S.F. Cauley, J.P. Stockmann, C.R. Sappo, et al., External dynamic interference estimation and removal (EDITER) for low field MRI, Magn. Reson. Med 87 (2022) 614–628.

[53] R. Kimmich, E. Anoardo, Field-cycling NMR relaxometry, Prog. Nucl. Magn. Reson. Spectrosc 44 (2004) 257–320.

[54] M.E. Halse, A. Coy, R. Dykstra, C. Eccles, et al., A practical and flexible implementation of 3D MRI in the Earth's magnetic field, J. Magn. Reson. 182 (2006) 75–83.

[55] C.A. Michal, Low-cost low-field NMR and MRI: Instrumentation and applications, J. Magn. Reson. 319 (2020), 106800.

[56] E.J.R. van Beek, C. Kuhl, Y. Anzai, P. Desmond, R.L. Ehman, Q. Gong, V. Gulani, M. Hall-Craggs, T. Leiner, C.C. Tschoyoson Lim, J.G. Pipe, S. Reeder, C. Reinhold, M. Smits, D.K. Sodickson, C. Tempany, H.A. Vargas, M. Wang, Value of MRI in medicine: more than just another test? J. Magn. Reson. Imag. (2018) https://doi.org/10.1002/jmri.26211.

[57] Y. Anzai, S. Minoshima, V.S. Lee, Enhancing value of MRI: a call for action, J. Magn. Reson. Imag. (2018), https://doi.org/10.1002/jmri.26239.

[58] O. Kraff, M.E. Ladd, MR safety update 2015: where do the risks come from? Curr. Radiol. Rep. 4 (2016) https://doi.org/10.1007/s40134-016-0163-y. DOI.

[59] Y.T. Araya, F. Martínez-Santisteban, W.B. Handler, C.T. Harris, B.A. Chronik, T. J. Scholl, Nuclear magnetic relaxation dispersion of murine tissue for development of T1 (R1) dispersion contrast imaging, NMR Biomed 30 (2017), https://doi.org/10.1002/nbm.3789.

[60] R. Kimmich (Ed.), New Developments in NMR: Field-cycling NMR Relaxometry. Instrumentation, Model Theories and Applications, Royal Society of Chemistry, Cambridge, UK, 2019.

[61] M. Flämig, M. Hoffmann, A. Lichtinger, E. A Rössler, Application of proton field-cycling NMR relaxometry for studying translational diffusion in simple liquids and polymer melts, Magn. Reson. Chem. 57 (2019) 805–817.

[62] E.G. Ates, V. Domenici, M. Florek-Wojciechowska, A. Gradišek, et al., Field-dependent NMR relaxometry for food science: applications and perspectives, Trends Food Sci. Technol. 110 (2021) 513–524.

[63] G. Parigi, E. Ravera, M. Fragai, C. Luchinat, Unveiling protein dynamics in solution with field-cycling NMR relaxometry, Prog. Nucl. Magn. Reson. Spectrosc. 124–125 (2021) 85–98.

[64] C.C. Fraenza, S.G. Greenbaum, Broadband NMR relaxometry of electrolytes for energy storage, Chem. Phys. Rev. 3 (2022), 011307.

[65] T. Apih, A. Gregorovič, V. Žagar, J. Seliger, A rapid determination of nuclear quadrupole resonance frequencies using field-cycling magnetic resonance and frequency modulated RF excitations, J. Magn. Reson. 310 (2020), 106635.

[66] B. Gizatullin, C. Mattea, S. Stapf, Field-cycling NMR and DNP – a friendship with benefits, J. Magn.Reson. 322 (2021), 106851.

[67] M. Bödenler, L. de Rochefort, P.J. Ross, N. Chanet, et al., Comparison of fast field-cycling magnetic resonance imaging methods and future perspectives, Mol. Phys. 117 (2019) 832–848.

[68] E. Anoardo, S. Kruber, G.O. Forte, G.A. Dominguez, New trends in field-cycling NMR technology, in: R. Kimmich (Ed.), Field-cycling NMR Relaxometry: Instrumentation, Model Theories and Applications, Royal Society of Chemistry, London, 2019, pp. 67–87.

[69] J.A. Romero, G.G. Rodriguez, E. Anoardo, A fast field-cycling MRI relaxometer for physical contrasts design and pre-clinical studies in small animals, J. Magn. Reson. 311 (2020), 106682.

[70] G.G. Rodriguez, E. Anoardo, Proton double irradiation field-cycling nuclear magnetic resonance imaging: testing new concepts and calibration methods, IEEE. Trans. Instrum. Meas. 70 (2020), https://doi.org/10.1109/TIM.2020.3037304.

[71] K.H. Schweikert, R. Krieg, F. Noack, A high-field air-cored magnet coil design for fast-field-cycling NMR, J. Magn. Reson. 78 (1988) 77–96.

[72] S.V. Dvinskikh, Y.V. Molchanov, S.R. Fillipov, Magnetic system for NMR relaxation-meter with field cycling, Prib. Teckh. Eksp. 21 (1988) 165–167.
[73] E. Anoardo, G. Galli, G. Ferrante, Fast-field-cycling NMR: applications and instrumentation, Appl. Magn. Reson. 20 (2001) 365–404.
[74] O Lips, A.F. Privalov, S.V. Dvimskik, F. Fujara, Magnet design with high b_0 homogeneity for fast-field-cycling NMR applications, J. Magn. Reson. 149 (2001) 22–28.
[75] S. Kruber, G. Farrher, E. Anoardo, Comparative study of helical-cut notch–coil magnets for fast-field-cycling nuclear magnetic resonance, Can. J. Phys. 92 (2014) 1430–1440.
[76] S. Kruber, G. Farrher, E. Anoardo, Air core notch-coil magnet with variable geometry for fast-field-cycling NMR, J. Magn. Reson. 259 (2015) 216–224.
[77] D.M. Sousa, G.D. Marques, J.M. Cascais, P.J. Sebastião, Desktop fast-field cycling nuclear magnetic resonance relaxometer, Solid State Nucl. Magn.Reson. 38 (2010) 36–43.
[78] Romero J. A. , PhD. Thesis, Universidad Nacional de Córdoba, Córdoba - Argentina, 2018.
[79] S.E. Ungersma, N.I. Matter, J.W. Hardy, R.D. Venook, et al., Magnetic resonance imaging with T1 dispersion contrast, Magn. Reson. Med. 55 (2006) 1362–1371.
[80] G.R. Davies, D.J. Lurie, Quantitative field-cycling T_1dispersion imaging, in: Proceeding of the ISMRM 13th Scientific Meeting, Miami – USA, 2005, p. 2187.
[81] M. Petit, M. Leclercq, S. Pierre, M.R. Ruggiero, et al., Fast-field-cycling NMR at very low magnetic fields: water molecular dynamic biomarkers of glioma cell invasion and migration, NMR Biomed 35 (2022), e4677.
[82] H. Utsumi, T. Masumizu, R. Kobayashi, T. Tahira, et al., Development and preclinical study of free radical imaging using field-cycling dynamic nuclear polarization MRI, Anal. Chem. 93 (2021) 14138–14145.
[83] P.T. Vesanen, J.O. Nieminen, K.C.J Zevenhoven, R.J.Ilmoniemi Y.-C.Hsu, Current-density imaging using ultra-low-field MRI with zero-field encoding, Magn. Reson. Imag. 32 (2014) 766–770.
[84] H. Chang, M. Fitzpatrick, A technique for accurate magnetic resonance imaging in presence of field inhomogeneities, IEEE Trans. Med. Imag. 11 (1992) 319–329.
[85] L.M. Broche, P.J. Ross, G.R. Davies, D.J. Lurie, Simple algorithm for the correction of MRI image artifacts due to random phase fluctuations, Magn. Reson. Imag. 44 (2017) 55–59.